Research Square

Preprints are preliminary reports that have not undergone peer review.
They should not be considered conclusive, used to inform clinical practice,
or referenced by the media as validated information.

Nanoscale 0.94NBT–0.06BT near the Morphotropic Phase Boundary: Hydrothermal Design and Enhanced Ferroelectric Energy Conversion

Lakshman Shaik
GITAM (Deemed to be University)
Ch. Jagadeesh
Vignan's Institute of Engineering for Women (A)
M. Sudha
Dr. V.S. Krishna Govt. Degree(A) & P.G. College
R. Neeraja
Nalla Narasimha Reddy Education Society's Group of Institutions Integrated Campus
P. H.K. Charan
Aditya Institute of Technology and Management
M. Ramanaiah
ramanaiahmalla4@gmail.com

Aditya Institute of Technology and Management

Research Article

Keywords: Sodium Bismuth Titanate–Barium Titanate solid solution, hydrothermal synthesis, lead-free ferroelectric ceramics, Morphotropic Phase Boundary, Polyvinylidene fluoride composites, ferroelectric properties, energy harvesting, flexible nanocomposites

Posted Date: June 5th, 2026

DOI: https://doi.org/10.21203/rs.3.rs-9698796/v1

License: This work is licensed under a Creative Commons Attribution 4.0 International License.
Read Full License

Additional Declarations: No competing interests reported.

Version of Record: A version of this preprint was published at Journal of Materials Science: Materials in Electronics on September 11th, 2026. See the published version at https://doi.org/10.1007/s10854-026-

18423-1.

Abstract

Lead-free ferroelectric nanomaterials have attracted considerable interest for sustainable electronic and energy harvesting technologies. In this work, 0.94NBT–0.06BT nanoparticles were synthesized via a hydrothermal method and incorporated into a flexible Polyvinylidene fluoride (PVDF) matrix to fabricate a high-performance ferroelectric composite. X-ray diffraction confirmed the formation of a pure perovskite phase, while Rietveld refinement revealed the coexistence of rhombohedral (R3c) and tetragonal (P4mm) structures near the Morphotropic Phase Boundary region. Raman spectroscopy further verified the distorted lattice through characteristic TiO_6 vibrational modes. FESEM analysis showed uniformly distributed nanoparticles with an average size of ~ 167 nm and homogeneous dispersion within the PVDF matrix. The material exhibited strong ferroelectric behavior with a maximum polarization of 40 $\mu C/cm^2$, remanent polarization of 33 $\mu C/cm^2$, and coercive field of 26 kV/cm. The composite demonstrated promising energy harvesting capability, generating an open-circuit voltage of 4.47 V and a maximum power output of 2.57 μW at 35 Hz, highlighting its potential for flexible self-powered electronic devices.

1. Introduction

The increasing demand for environmentally sustainable electronic materials has stimulated extensive research on lead-free ferroelectric ceramics for next-generation electromechanical and energy conversion devices [1–3]. Conventional ferroelectric materials such as lead zirconatetitanate (PZT) exhibit excellent piezoelectric and ferroelectric properties; however, the presence of toxic lead poses serious environmental and health concerns [4–5]. As a result, significant efforts have been directed toward developing alternative lead-free ferroelectric systems with comparable functional performance. Among various candidates, perovskite-based materials derived from Sodium Bismuth Titanate ($Na_{0.5}Bi_{0.5}TiO_3$, NBT) have emerged as promising substitutes due to their large spontaneous polarization, relatively high Curie temperature, and strong ferroelectric response [6–7]. These characteristics make NBT-based materials attractive for applications in sensors, actuators, and energy harvesting systems.

In particular, the solid solution formed between Sodium Bismuth Titanate and Barium Titanate has gained considerable attention because of its enhanced electrical and electromechanical performance near the Morphotropic Phase Boundary (MPB). At compositions close to the MPB, the coexistence of rhombohedral and tetragonal phases promotes polarization rotation and domain mobility, which significantly improves the dielectric, ferroelectric, and piezoelectric responses of the material [8–9]. Among these compositions, 0.94NBT–0.06BT has been widely recognized as an optimized composition that exhibits improved structural flexibility and enhanced functional properties [10–11]. Such characteristics make this system particularly suitable for the development of high-performance lead-free ferroelectric devices.

Despite significant progress in the development of NBT–BT ceramics, several research challenges still remain. Most reported studies rely on conventional solid-state synthesis techniques, which generally require high processing temperatures and often produce materials with large grain sizes and non-uniform microstructures. These limitations can restrict domain wall motion and reduce the overall functional performance of the material. Furthermore, limited studies have explored the synthesis of nanoscale NBT–BT particles via hydrothermal methods and their integration into flexible polymer matrices for advanced energy harvesting applications [12–13]. Therefore, a clear research gap exists in understanding how hydrothermally synthesized NBT–BT nanoparticles can be effectively utilized to enhance ferroelectric properties and improve the performance of flexible composite systems.

To address these challenges, the present work focuses on the hydrothermal synthesis of 0.94NBT–0.06BT nanoparticles and their incorporation into a polymer matrix based on Polyvinylidene fluoride (PVDF) to develop a flexible ferroelectric composite [13–14]. The main objectives of this study are: (i) to synthesize highly crystalline NBT–BT nanoparticles with controlled nanoscale morphology using a hydrothermal technique, (ii) to investigate their structural and lattice characteristics using X-ray diffraction, Rietveld refinement, and Raman spectroscopy, (iii) to analyze the microstructural features and particle dispersion using FESEM, and (iv) to evaluate the ferroelectric behavior and energy harvesting performance of the resulting composite system. By achieving these objectives, this work aims to provide a deeper understanding of the relationship between nanoscale structure and functional performance in lead-free ferroelectric composites.From an application perspective, the development of flexible NBT–BT/PVDF composites is particularly important for emerging industrial technologies. Such materials can efficiently convert low-frequency mechanical vibrations into electrical energy, enabling their use in self-powered sensors, wearable electronics, biomedical monitoring devices, and industrial vibration energy harvesting systems. In addition, their lead-free composition and high polarization capability make them environmentally friendly alternatives to conventional piezoelectric materials used in smart devices and energy storage components. Therefore, the findings of the present work not only contribute to the fundamental understanding of nanoscale NBT–BT ferroelectrics but also highlight their potential for sustainable industrial applications in next-generation electronic and energy harvesting technologies.

2. Experimental Procedure

Lead-free $0.94(Na_{0.5}Bi_{0.5})TiO_3–0.06BaTiO_3$(0.94NBT–0.06BT) nanoparticles were synthesized via a hydrothermal technique using high-purity analytical reagents. Sodium hydroxide (NaOH, ≥ 99%, Merck), bismuth nitrate pentahydrate [$Bi(NO_3)_3·5H_2O$, ≥ 99.9%, Sigma-Aldrich], barium nitrate [$Ba(NO_3)_2$, ≥ 99%, Merck], and titanium isopropoxide [$Ti(OCH(CH_3)_2)_4$, 97%, Sigma-Aldrich] were used as starting precursors without further purification. Initially, stoichiometric quantities of $Bi(NO_3)_3·5H_2O$ and $Ba(NO_3)_2$ corresponding to the desired composition were dissolved separately in deionized water under continuous magnetic stirring to form homogeneous solutions. Titanium isopropoxide was then slowly introduced into the mixed solution under vigorous stirring to avoid premature hydrolysis and to ensure

uniform precursor mixing. Subsequently, a concentrated NaOH solution was added dropwise to adjust the pH of the reaction medium to approximately pH ≈ 12, which is favorable for the nucleation of the perovskite phase. The resulting precursor mixture was transferred into a 100 mL Teflon-lined stainless-steel autoclave and sealed tightly. The hydrothermal reaction was carried out at 180°C for 12 h in a programmable oven. After completion of the reaction, the autoclave was allowed to cool naturally to room temperature. The obtained precipitate was repeatedly washed with deionized water and ethanol several times to remove residual ions and impurities, followed by centrifugation at 5000 rpm for 10 min. The purified powder was then dried in a hot-air oven at 80°C for 10 h to obtain fine 0.94NBT–0.06BT nanoparticles.

- **Fabrication of 0.94NBT–0.06BT/PVDF Composite Film**:

To fabricate flexible composite films, the synthesized nanoparticles were incorporated into a polymer matrix of polyvinylidene fluoride (PVDF). PVDF pellets (Mw ≈ 534,000, Sigma-Aldrich, ≥ 99%) were dissolved in N,N-dimethylformamide (DMF, ≥ 99.8%, Merck) under constant magnetic stirring at 60°C for 2 h to obtain a clear polymer solution. A calculated amount of the synthesized 0.94NBT–0.06BT nanoparticles was dispersed into the PVDF solution and subjected to ultrasonication for 30 min to ensure homogeneous dispersion of the ceramic fillers. The resulting suspension was then cast onto a clean glass substrate using a doctor blade technique and dried at 70°C for 12 h to remove the solvent completely, forming flexible 0.94NBT–0.06BT/PVDF composite films.The phase formation and crystal structure of the synthesized nanoparticles were analyzed using X-ray diffraction (XRD) on a RigakuMiniFlex 600 diffractometer with Cu Kα radiation (λ = 1.5406 Å) operated at 40 kV and 30 mA over a 2θ range of 20°–80° with a scanning rate of 2° min^{-1}. Structural refinement of the diffraction data was carried out using the Rietveld refinement method with FullProf software. Raman spectroscopy was performed using a RenishawinVia Raman spectrometer equipped with a 532 nm excitation laser, recorded in the spectral range of 100–900 cm^{-1} to examine lattice vibrations and local structural distortions. The surface morphology and particle size distribution were investigated using field emission scanning electron microscopy (FESEM, JEOL JSM-7600F) operated at an accelerating voltage of 10 kV. The ferroelectric properties were measured using a Radiant Technologies Precision Premier II ferroelectric tester, where polarization–electric field (P–E) hysteresis loops were recorded at an applied electric field of 60 kV cm^{-1}. The energy harvesting performance of the composite film was evaluated by measuring the generated output voltage and current under periodic mechanical vibrations using a digital storage oscilloscope (Tektronix TBS 1102B) and a low-frequency mechanical vibration setup operating around 35 Hz.

The working principle and structural design of the flexible 0.94NBT–0.06BT/PVDF piezoelectric nanogenerator (PENG) are illustrated in the provided schematic. The device assembly features an active piezoelectric layer comprising the synthesized 167 nm ceramic nanoparticles embedded within a PVDF matrix sandwiched between conductive electrodes on a flexible substrate. The operational mechanism is rooted in the transition of internal dipoles: in the initial state, the dipoles are randomly oriented; however, upon the application of a poling field, they align to create a macroscopic polarization.As

depicted in the mechanical-to-electrical conversion cycle, the absence of external pressure maintains electrical equilibrium. When mechanical stress is applied via a controlled setup—consisting of a voltage generator, a mechanical shaker, and an oscilloscope—the resulting deformation of the active layer disturbs the dipole equilibrium, generating a piezoelectric potential that drives an external flow of electrons. Upon the release of pressure, the dipoles return to their original state, producing a reverse current pulse. This cyclic process facilitates the conversion of kinetic energy into a stable electrical output, achieving a peak performance of 4.4697 V at a resonant frequency of 35 Hz. The Real Image of nanogenerator demonstrates the excellent flexibility of the fabricated device, confirming its potential for integration into wearable and conformable energy-scavenging systems presents in Fig. 1.

3. Results and Discussion

The crystal structure of the hydrothermally synthesized $0.94(Na_{0.5}Bi_{0.5})TiO_3–0.06BaTiO_3$(0.94NBT–0.06BT) nanoparticles was analyzed using X-ray diffraction (XRD), and the obtained pattern is illustrated in Fig. 2. The diffraction profile demonstrates the formation of a well-defined perovskite phase with no detectable secondary phases, indicating that the hydrothermal process successfully produced a phase-pure material. The major diffraction peaks appear at approximately $2\theta \approx 22°$, 32°, 39°, 46°, 51°, 57°, 67°, and 77°, which correspond to the pseudocubic lattice planes $(100)_{PC}$, $(110)_{PC}$, $(111)_{PC}$, $(200)_{PC}$, $(210_{PC}$, $(211)_{PC,}$$(300)_{PC}$and $(310)_{PC}$respectively. These reflections match well with the typical perovskite structures of Sodium Bismuth Titanate and Barium Titanate, confirming the successful incorporation of $BaTiO_3$ into the NBT lattice to form a homogeneous solid solution. The intense diffraction peak corresponding to the $(110)_{PC}$plane near 32° reflects the good crystallinity of the nanoparticles. In addition, the moderate broadening of the peaks suggests that the synthesized particles possess nanoscale crystallite dimensions. The group of reflections observed between 39° and 46° indicates slight lattice distortion and possible coexistence of different structural symmetries, implying that the composition lies close to the Morphotropic Phase Boundary (MPB) region of the NBT–BT system [15–16]. Such structural characteristics are often associated with enhanced electromechanical behavior in lead-free ferroelectric ceramics. Overall, the XRD analysis verifies that the hydrothermal route enables the preparation of 0.94NBT–0.06BT nanoparticles with a stable perovskite framework and nanoscalecrystallinity, making them promising candidates for advanced lead-free ferroelectric applications.

The crystal structure of the hydrothermally synthesized 0.94NBT–0.06BT nanoparticles was further investigated through structural refinement of the X-ray diffraction data using the Rietveld Refinement approach, and the refined profile is displayed in Fig. 3. The calculated diffraction pattern shows very close agreement with the measured data over the entire diffraction range, while the difference profile remains small, confirming the suitability of the refinement model. The refinement produced low reliability factors with R_P = 1.87%, R_{WP} = 4.01%, and χ^2 = 1.91, indicating a satisfactory fit between the observed and simulated patterns.The analysis reveals that the material consists of two coexisting crystallographic phases corresponding to rhombohedral (R3c) and tetragonal (P4mm) symmetries, with estimated phase

contributions of approximately 81% and 19%, respectively. This mixed structural state suggests that the composition lies close to the Morphotropic Phase Boundary (MPB) region, which is known to promote enhanced electromechanical behavior in lead-free ferroelectric systems. The enlarged views of the diffraction peaks around $2\theta \approx 32°$ and 46° show slight asymmetry and subtle peak separation, providing additional evidence for the coexistence of two structural symmetries. The structural modification can be attributed to the incorporation of Ba^{2+} ions into the A-site lattice positions of the perovskite framework derived from Sodium Bismuth Titanate and Barium Titanate, which induces lattice distortion and stabilizes the mixed-phase structure. Overall, the refinement results verify that the hydrothermal synthesis route yields highly crystalline 0.94NBT–0.06BT nanoparticles with a stable mixed rhombohedral–tetragonal perovskite structure, characteristic of compositions located near the MPB region.

The vibrational properties and local structural features of the hydrothermally synthesized 0.94NBT–0.06BT nanoparticles were examined using Raman spectroscopy, and the spectrum is presented in Fig. 4. The Raman profile shows several broad vibrational bands distributed between 100 and 900 cm^{-1}, indicating the presence of a distorted perovskite lattice. A noticeable Raman band appears around ~ 140 cm^{-1}, which is associated with lattice vibrations of the A-site cations in the perovskite framework formed from Sodium Bismuth Titanate and Barium Titanate. Another intense and broad feature centered near ~ 280–300 cm^{-1} can be attributed to bending motions and tilting of the TiO_6 octahedral units within the crystal structure.Additional Raman bands are visible in the intermediate frequency region at approximately ~ 520 cm^{-1} and ~ 590 cm^{-1}, which correspond to stretching vibrations of the Ti–O bonds in the oxygen octahedral [17–18]. These modes reflect distortions in the local lattice environment. At higher wavenumbers, relatively weak bands appear around ~ 730 cm^{-1}, ~ 800 cm^{-1}, and ~ 860 cm^{-1}, which are related to higher-order Ti–O stretching vibrations and oxygen lattice modes. The broad and overlapping nature of these Raman peaks suggests the presence of local structural disorder and nanoscale lattice distortions within the material. Such spectral behavior is commonly observed in solid-solution ferroelectric systems located near the Morphotropic Phase Boundary (MPB) region. Overall, the Raman analysis indicates that the synthesized 0.94NBT–0.06BT nanoparticles exhibit a distorted perovskite structure with complex lattice vibrations, supporting the structural information obtained from the X-ray diffraction and refinement studies.

The microstructural evolution and surface topography of the hydrothermally processed 0.94NBT–0.06BTnanoparticles, along with their integration into a polymer matrix, are illustrated in Fig. 5 As shown in the FESEM micrograph in Fig. 5**(a)**, the powder consists of a combination of near-spherical and irregularly shaped grains. While the high surface energy inherent to ferroelectric nanopowders leads to some interparticle clustering, the individual grain boundaries remain distinct, suggesting that the hydrothermal conditions were well-optimized for discrete nucleation. This is further supported by the statistical analysis in Fig. 5**(b)**, where a Gaussian fit of the particle size distribution identifies a mean diameter of approximately 167 nm. The majority of the particles are concentrated within a narrow sub-micron range, which aligns with the crystallite dimensions typically derived from XRD peak

broadening.The effectiveness of incorporating these ceramic fillers into a flexible framework is demonstrated by comparing the smooth, featureless surface of the pristine PVDF (Fig. 5c) with the PVDF-0.94NBT-0.06BT composite (Fig. 5d). In the composite image, the 0.94NBT–0.06BT nanoparticles appear as high-contrast bright inclusions uniformly embedded within the darker polymer medium. The lack of large-scale agglomerates in the composite indicates a successful dispersion process, which is critical for minimizing localized stress and maximizing the dielectric response [19–20]. This refined nanoscale morphology, characterized by a consistent 167 nm grain size and homogeneous distribution, provides the high surface-to-volume ratio necessary to enhance polarization dynamics and improve the overall electrical performance of the ferroelectric system.

The ferroelectric response of the hydrothermally synthesized 0.94NBT–0.06BT nanoparticles is characterized by the polarization-electric field (P-E) hysteresis loop and the corresponding switching current (I-E) profile shown in the provided figure. At a peak applied field of 60 kV/cm, the material displays a robust, well-saturated hysteresis loop, yielding a maximum polarization (P_{max}) of approximately 40μC/cm^2. The remanent polarization (P_r) is notably high at 33 μC/cm^2, indicating a strong retention of dipole alignment once the external field is removed. The coercive field (E_C), which defines the threshold for domain reversal, is found to be approximately 26 kV/cm.The validity of this ferroelectric switching is further supported by the bipolar switching current (I-E) peaks (represented by the dashed lines), which are sharply centered at the coercive field values. These current transients confirm that the polarization is derived from the reorientation of ferroelectric domains rather than being an artifact of leakage or resistive effects. Such prominent $P_r$and P_{max} values in particles with a mean size of 167 nm suggest that the hydrothermal process successfully minimizes crystalline defects that typically clamp domain wall motion. Consequently, this composition demonstrates the high dielectric performance required for integration into functional NBT-BT-based composite systems.

The microstructural landscape and chemical footprint of the 0.94NBT–0.06BT/PVDF system highlight its potential as a high-performance, lead-free functional material. FESEM analysis confirms the successful synthesis of sub-micron particles with a mean diameter of 167 nm, exhibiting a controlled geometry that prevents the deleterious effects of overgrowth. When incorporated into the PVDF matrix, these nanoparticles serve as nucleating agents for the electroactiveβ-phase, as validated by the 840cm^{-1}and 1275 cm^{-1}bands in the FTIR spectra. The resulting composite maintains a high degree of phase purity and homogeneity, which is essential for uniform stress distribution and efficient mechanical-to-electrical conversion.The macroscopic performance of the material is rooted in its robust ferroelectric properties. At a peak electric field of 60 kV/cm, the composition yields a significant remanentpolarization (P_r) of 33 μC/cm^2 and a maximum polarization (P_{max}) of 40 μC/cm^2. These values, coupled with distinct switching current peaks at a coercive field of 26 kV/cm, demonstrate that the 167 nm grains maintain high domain mobility despite their reduced size. This strong polarization directly translates into superior energy harvesting capabilities; the composite generates a stable open-circuit voltage of 4.4697 V at an optimal frequency of 35 Hz. With a recorded peak power output of 2.57 μW and a short-circuit current of 1.12 μA the system proves highly efficient at capturing energy from low-frequency mechanical vibrations.The

practical implications of these findings are extensive in the realm of sustainable electronics. The biocompatible nature of the NBT-BT filler makes this composite an ideal candidate for self-powered biomedical devices, such as cardiac monitors or electronic skin, where the 1.12μA output can drive low-power diagnostic sensors. Furthermore, its resonance at 35 Hz makes it particularly suitable for industrial IoT applications, where it can harvest energy from machinery vibrations to power wireless telemetry units [21–22]. Additionally, the high P_{max} suggests a capacity for energy-dense capacitor applications, supporting the development of lead-free, high-pulse-power storage systems. Collectively, these results position the 0.94NBT–0.06BT$/PVDF composite as a versatile and eco-friendly platform for next-generation self-sustaining technologies.

4. Conclusions

The present study successfully demonstrates the synthesis and comprehensive characterization of 0.94NBT–0.06BT nanoparticles prepared via a hydrothermal route and their incorporation into a flexible polymer composite. X-ray diffraction analysis confirmed the formation of a single-phase perovskite structure, while structural refinement revealed the coexistence of rhombohedral (R3c) and tetragonal (P4mm) phases, indicating that the composition lies near the Morphotropic Phase Boundary (MPB) region. Raman spectroscopy further verified the distorted perovskite lattice through characteristic vibrational modes associated with TiO_6 octahedral bending and stretching. The FESEM analysis revealed uniformly distributed nanoparticles with an average particle size of approximately 167 nm, indicating successful control of morphology through the hydrothermal synthesis process. The homogeneous dispersion of these nanoparticles within the Polyvinylidene fluoride (PVDF) matrix confirmed the formation of a well-integrated composite structure.The ferroelectric measurements demonstrated a well-defined polarization–electric field hysteresis loop with a maximum polarization (P_{max}) of about 40 $\mu C/cm^2$, remanent polarization (P_r) of 33 $\mu C/cm^2$, and coercive field (E_C) of approximately 26 kV/cm, indicating strong ferroelectric behavior. The switching current peaks observed near the coercive field confirmed the intrinsic domain switching mechanism within the material. These strong polarization characteristics, combined with the nanoscale morphology of the particles, contribute significantly to the improved electromechanical response of the composite system.Furthermore, the fabricated 0.94NBT–0.06BT/PVDF composite exhibited promising energy harvesting performance, generating an open-circuit voltage of 4.4697 V, a short-circuit current of 1.12 μA, and a maximum power output of 2.57 μW under mechanical vibration at 35 Hz. These results demonstrate the ability of the composite to effectively convert low-frequency mechanical energy into electrical energy. The enhanced electrical output is attributed to the synergistic interaction between the ferroelectric ceramic nanoparticles and the flexible PVDF matrix, which facilitates efficient polarization and mechanical stress transfer.Overall, the combination of nanoscale structural control, strong ferroelectric response, and efficient energy harvesting capability highlights the potential of the 0.94NBT–0.06BT/PVDF composite as a sustainable and environmentally friendly functional material. The lead-free nature of the system makes it particularly attractive for practical applications in self-powered wearable electronics, biomedical sensing devices, flexible energy harvesters, and industrial vibration monitoring systems. Therefore, this work provides

valuable insights into the design of high-performance lead-free ferroelectric nanocomposites for next-generation energy conversion and smart electronic technologies.

Declarations

ACKNOWLEDGMENTS

RamanaiahMallathanks to Dr. MabuSubhan, Department of S@H, RGUKT Ongole, thanked for his assistance with structural refinement.

Data Availability

The authors declare thatall the data generated or analyzed during this study are included in this manuscript

Conflict of Interest

The authors declare that they have no conflict of interest.

CRediT authorship contribution statement:

LakshmanShaik: Conceptualization, methodology, investigation, data curation, formal analysis, and writing – original draft preparation. **Ch. Jagadeesh:** Methodology, investigation, and validation. M. **Suha:** Formal analysis, visualization, and writing – review and editing. **R. Neeraja:** Resources, investigation, and data validation. **P.H.K. Charan:** Software, visualization, and data interpretation. **M. Ramanaiah:** Supervision, project administration, funding acquisition, and writing – review and editing. All authors have read and approved the final manuscript.

Funding Statement

The authors declare that this research was conducted without any specific financial support from funding agencies, commercial, or not-for-profit organizations.

References

1. F. Li, B. Wang, X. Gao, D. Damjanovic, L.Q. Chen, S. Zhang, Ferroelectric materials toward next-generation electromechanical technologies. Science. **389**, eadn4926 (2025)
2. A. Akshayveer, F.C. Buroni, R. Melnik, L. Rodriguez-Tembleque, A. Saez, Environment-friendly technologies with lead-free piezoelectric materials: A review of recent developments, applications, and modelling approaches. arXiv. **2502**, 20250 (2025)

3. Z. Sun, Z. Wang, Y. Tian, G. Wang, W. Wang, M. Yang, Y. Pu, Progress, outlook, and challenges in lead-free energy-storage ferroelectrics. Adv. Electron. Mater. **6**, 1900698 (2020)
4. P.K. Panda, Environmental friendly lead-free piezoelectric materials. J. Mater. Sci. **44**, 5049–5062 (2009)
5. T. Ibn-Mohammed, I.M. Reaney, S.C.L. Koh, A. Acquaye, D.C. Sinclair, C.A. Randall, L. Ozawa-Meida, Life cycle assessment and environmental profile evaluation of lead-free piezoelectrics in comparison with lead zirconatetitanate. J. Eur. Ceram. Soc. **38**, 4922–4938 (2018)
6. K. Teki, H.S. Mohanty, K. Bhoi, S. Karmakar, H. Borkar, S. Mohapatra, Effect of vanadium doping on structural, vibrational, optical, dielectric and ferroelectric properties of $Na_{0.5}Bi_{0.5}TiO_3$ ceramics. J. Mater. Sci. : Mater. Electron. **36**, 1788 (2025)
7. C. Ma, X. Wang, W. Tan, W. Zhou, X. Wang, Z. Cheng, Z. Zhai, Enhanced photoluminescence and ferro/piezoelectric performance in piezo-luminescent materials. Dalton Trans. **49**, 5581–5589 (2020)
8. U. Shankar, N. Kumar, G. Ji, M.K. Singh, Comparative analysis of electromechanical performance of MPB and relaxor ferroelectrics. Mater. Today Commun. **42**, 111283 (2025)
9. E.B. Araújo, Recent advances in PMN–PT ferroelectric ceramics near MPB. in Adv. Ceram., 43–60 (2011)
10. K.S.K.R. Chandra Sekhar, M.L.V. Mahesh, T. Sreenivasu, Y. Rama Krishna, C. Mouli, K. and, P. Tirupathi, Structural evolution and dielectric relaxation in Dy-substituted NBT–BT ceramics. J. Mater. Sci. : Mater. Electron. **32**, 8628–8647 (2021)
11. M. Mesrar, T. Lamcharfı, N.S. Echatoui, F. Abdi, Crystal structure and piezoelectric properties of NBT–BT-based ceramics, *Heliyon*, 10, eXXXX (2024)
12. R.K. Razack, K.K. Sadasivuni, Advancing nanogenerators using 3D-printed nanocomposites. Polymers. **17**, 1367 (2025)
13. L.R. Devi, B.D. Naorem, A. Chowdhuri, B.S. Hidangmayum, Flexible PVDF/BST nanocomposites for energy harvesting. SSRN, 4839858 (2025)
14. S. Praharaj, D. Rout, Lead-free dielectrics for green energy storage, in *Adv. Nanostruct. Mater.*, Springer, 37–56 (2022)
15. Y.J. Dai, J.S. Pan, X.W. Zhang, Composition range of MPB in NBT–BT system. Key Eng. Mater. **336**, 206–209 (2007)
16. Q. Zhang, X. Zhao, R. Sun, H. Luo, Crystal growth and electrical properties of NBT–BT near MPB. Phys. Status Solidi A **208**, 1012–1020 (2011)
17. T.B.T. An, FT-Raman and FTIR studies of titanias. J. Chem. Soc. Faraday Trans. **90**, 3181–3190 (1994)
18. Z. Liu, R.J. Davis, Structure of Ti–Si mixed oxides by spectroscopic techniques. J. Phys. Chem. **98**, 1253–1261 (1994)

19. D.Q. Tan, Polymer-based nanodielectrics for advanced capacitors. Adv. Funct. Mater. **30**, 1808567 (2020)
20. C. Zhang, C. Yuan, Q. Zhu, H. Sun, Fabrication of PVDF piezoelectric composite films. Ceram. Int. **49**, 27255–27265 (2023)
21. M.H. Alsharif, S. Kim, N. Kuruoğlu, Energy harvesting techniques for wireless sensor networks. Symmetry. **11**, 865 (2019)
22. G. Moloudian, M. Hosseinifard, S. Kumar, R.B. Simorangkir, J.L. Buckley, C. Song, B. O'Flynn, RF energy harvesting for IoT applications. IEEE Sens. J. **24**, 5732–5745 (2024)

Figures

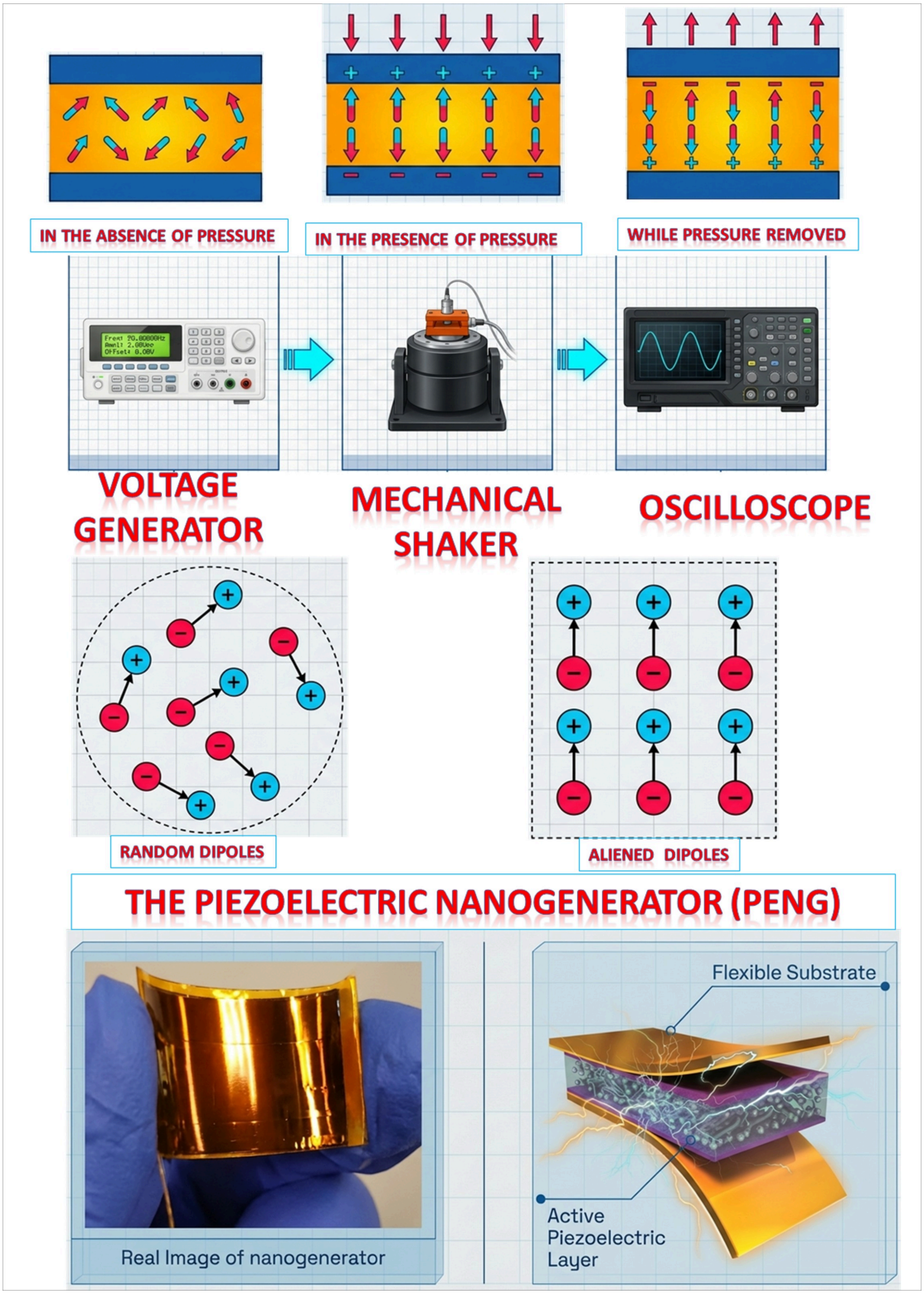


Figure 1

Schematic representation of the hydrothermal synthesis process for the preparation of 0.94NBT–0.06BT nanoparticles and their incorporation into the polymer matrix.

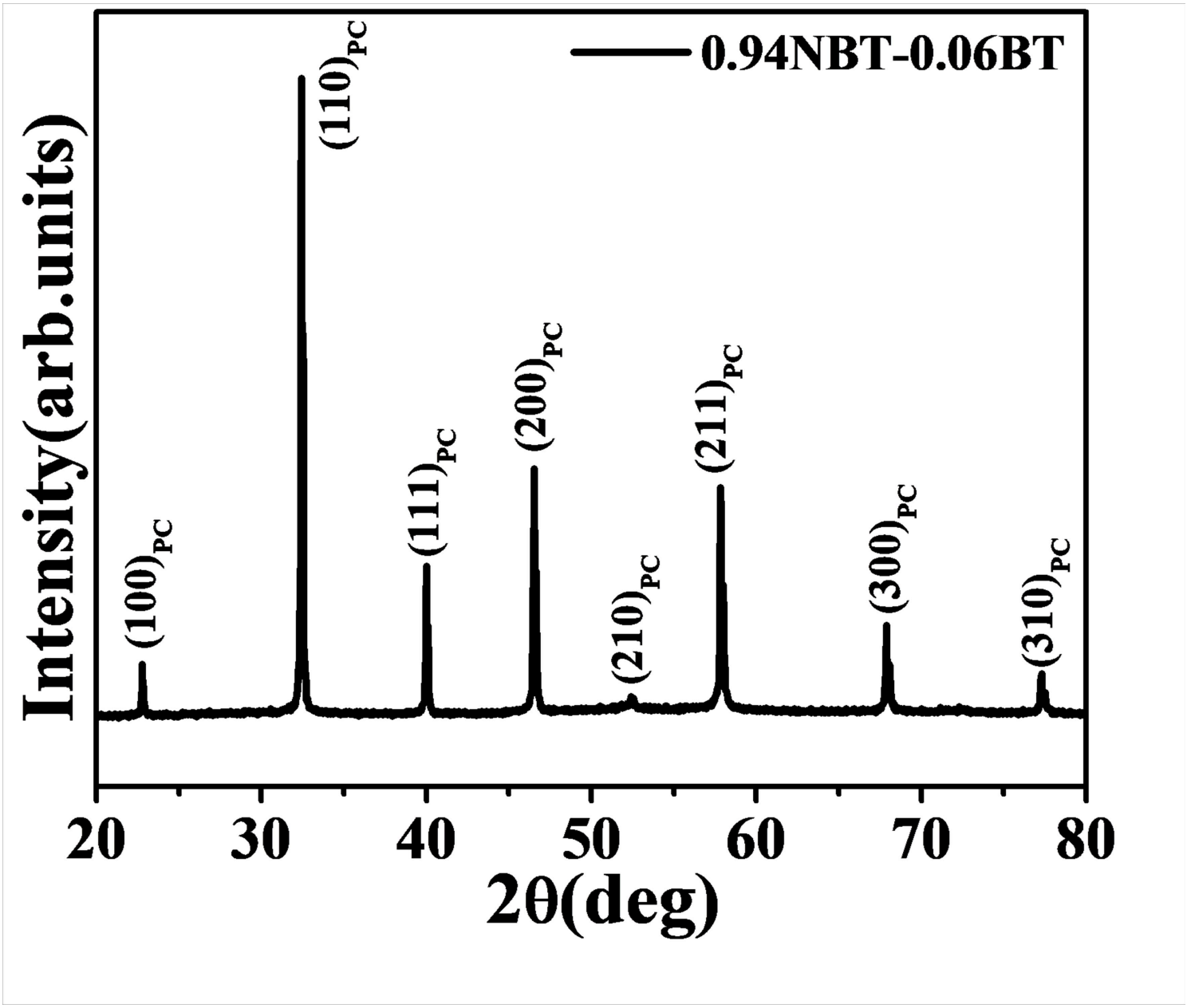


Figure 2

X-ray diffraction (XRD) pattern of hydrothermally synthesized 0.94NBT–0.06BT nanoparticles, showing the formation of a single-phase perovskite structure with indexed pseudocubic reflections.

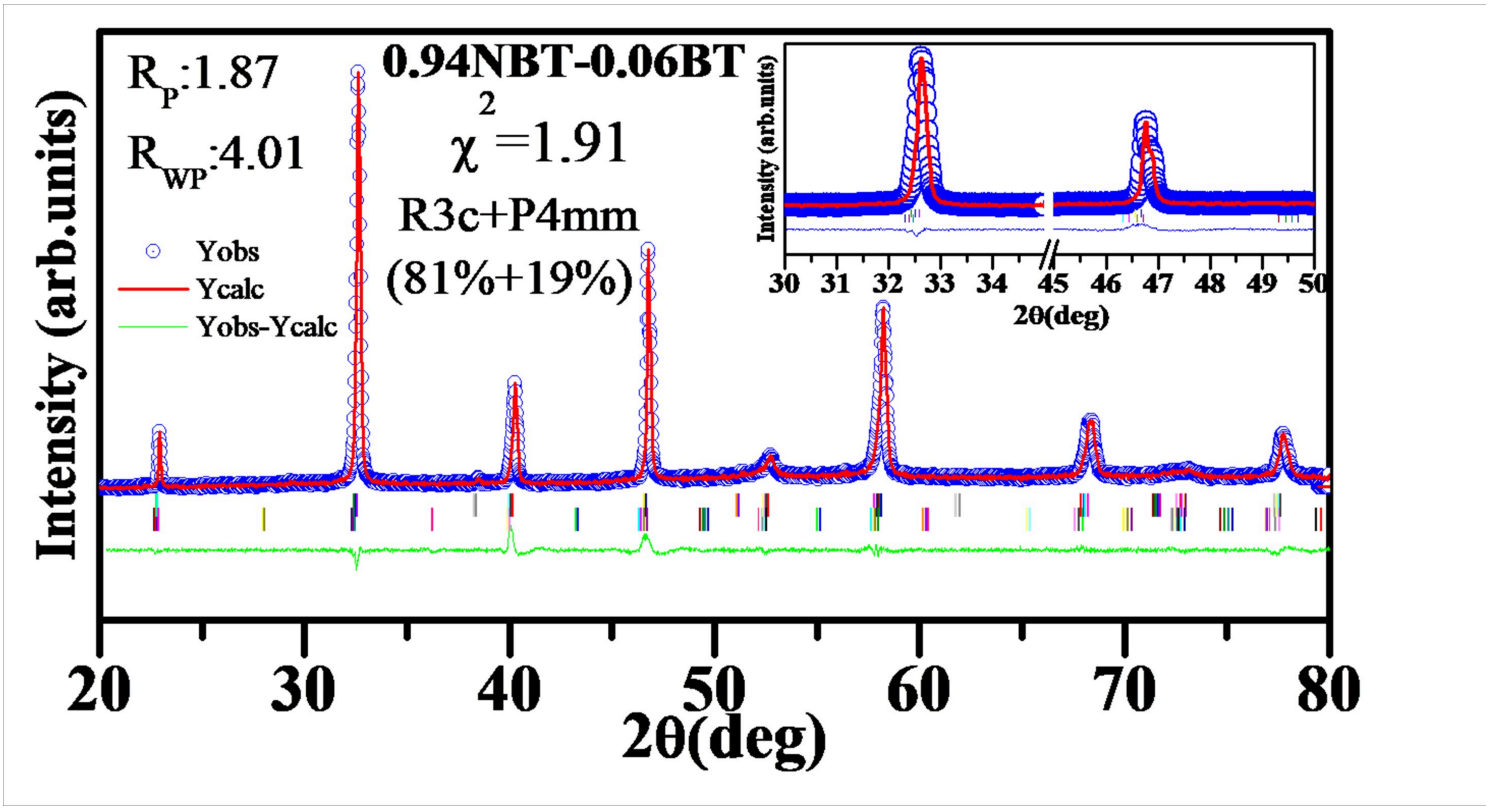


Figure 3

Rietveld refinement profile of the XRD data for 0.94NBT–0.06BT nanoparticles showing observed pattern (Y_{obs}), calculated pattern (Y_{calc}), Bragg reflection positions, and difference curve, confirming the coexistence of rhombohedral (R3c) and tetragonal (P4mm) phases.

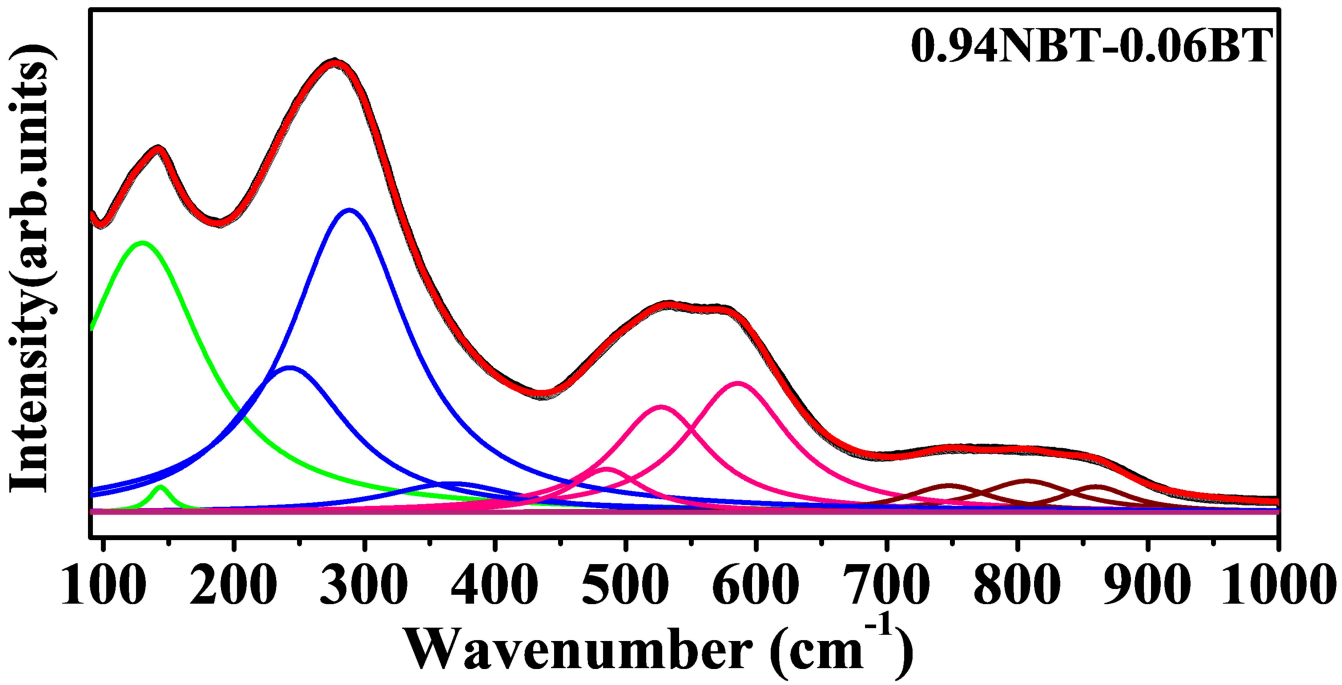


Figure 4

Raman spectrum of hydrothermally synthesized 0.94NBT–0.06BT nanoparticles, indicating characteristic lattice vibration modes associated with TiO_6 octahedral bending and stretching in the perovskite structure.

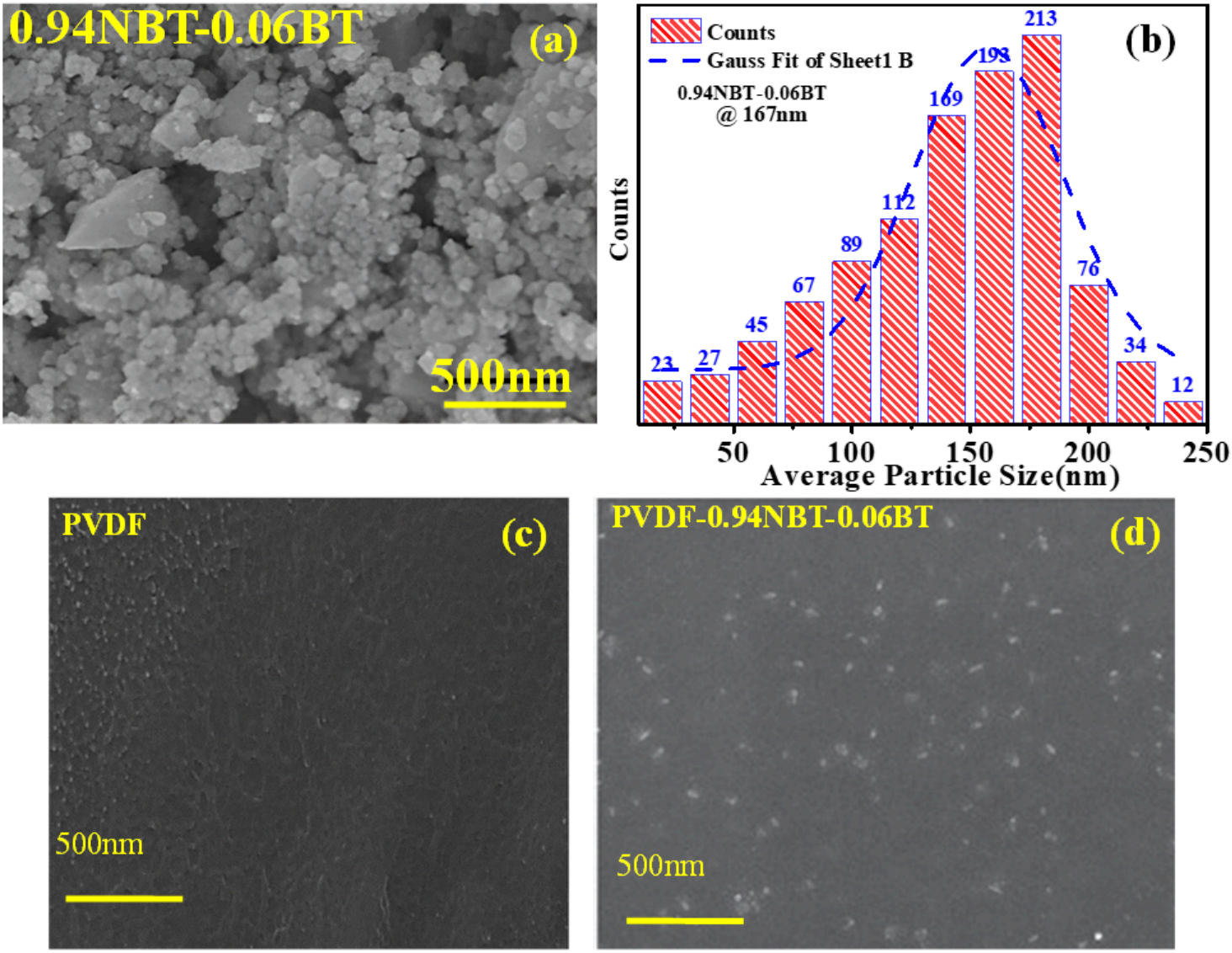


Figure 5

FESEM micrographs of (a) hydrothermally synthesized 0.94NBT–0.06BT nanoparticles, (b) particle size distribution with Gaussian fitting showing an average particle size of ~167 nm, (c) surface morphology of pristine Polyvinylidene fluoride (PVDF) film, and (d) FESEM image of 0.94NBT–0.06BT/PVDF composite showing uniform dispersion of nanoparticles within the polymer matrix.

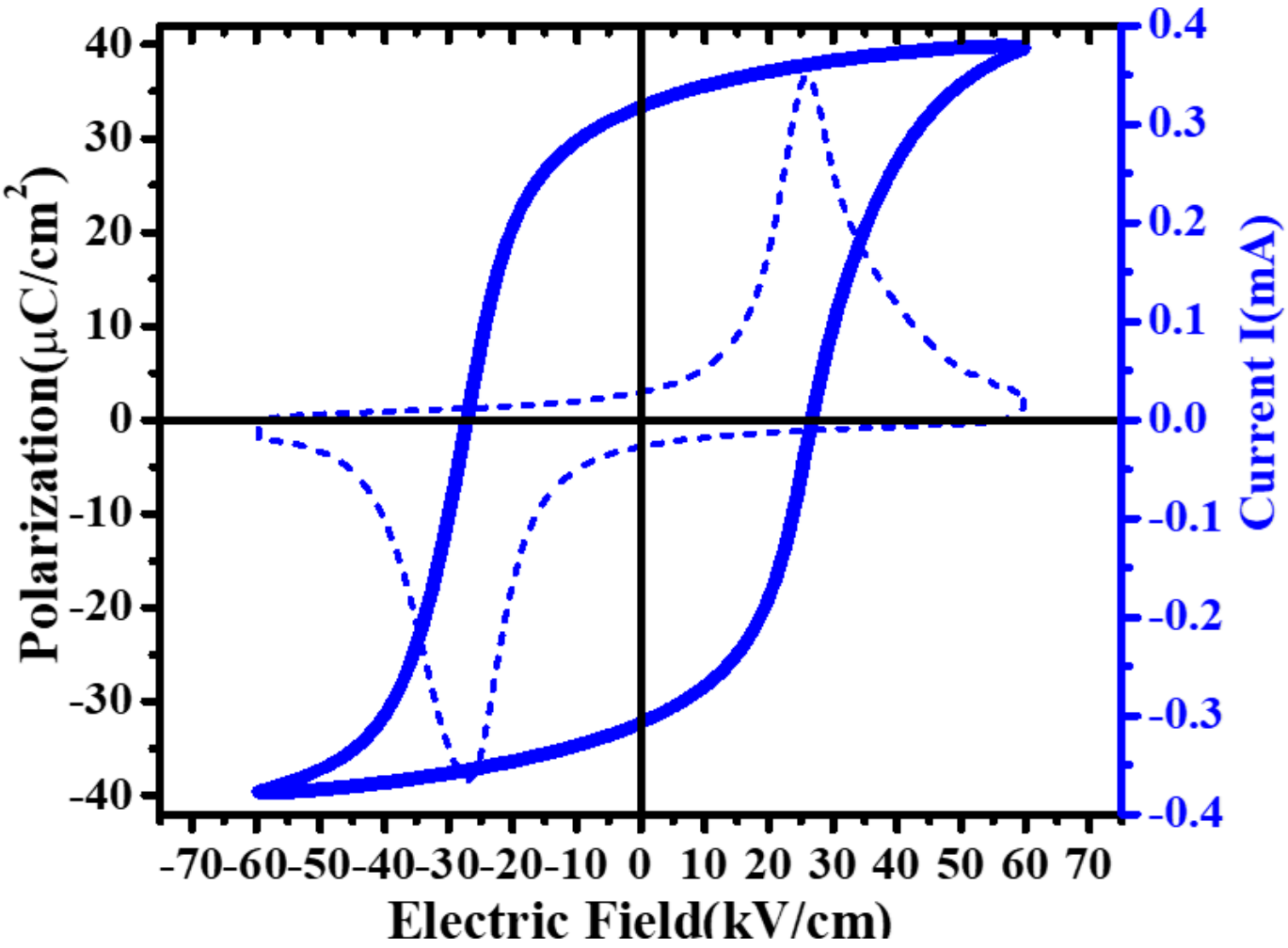


Figure 6

Polarization–electric field (P–E) hysteresis loop and corresponding switching current (I–E) characteristics of 0.94NBT–0.06BT nanoparticlesmeasured at an applied electric field of 60 kV/cm.

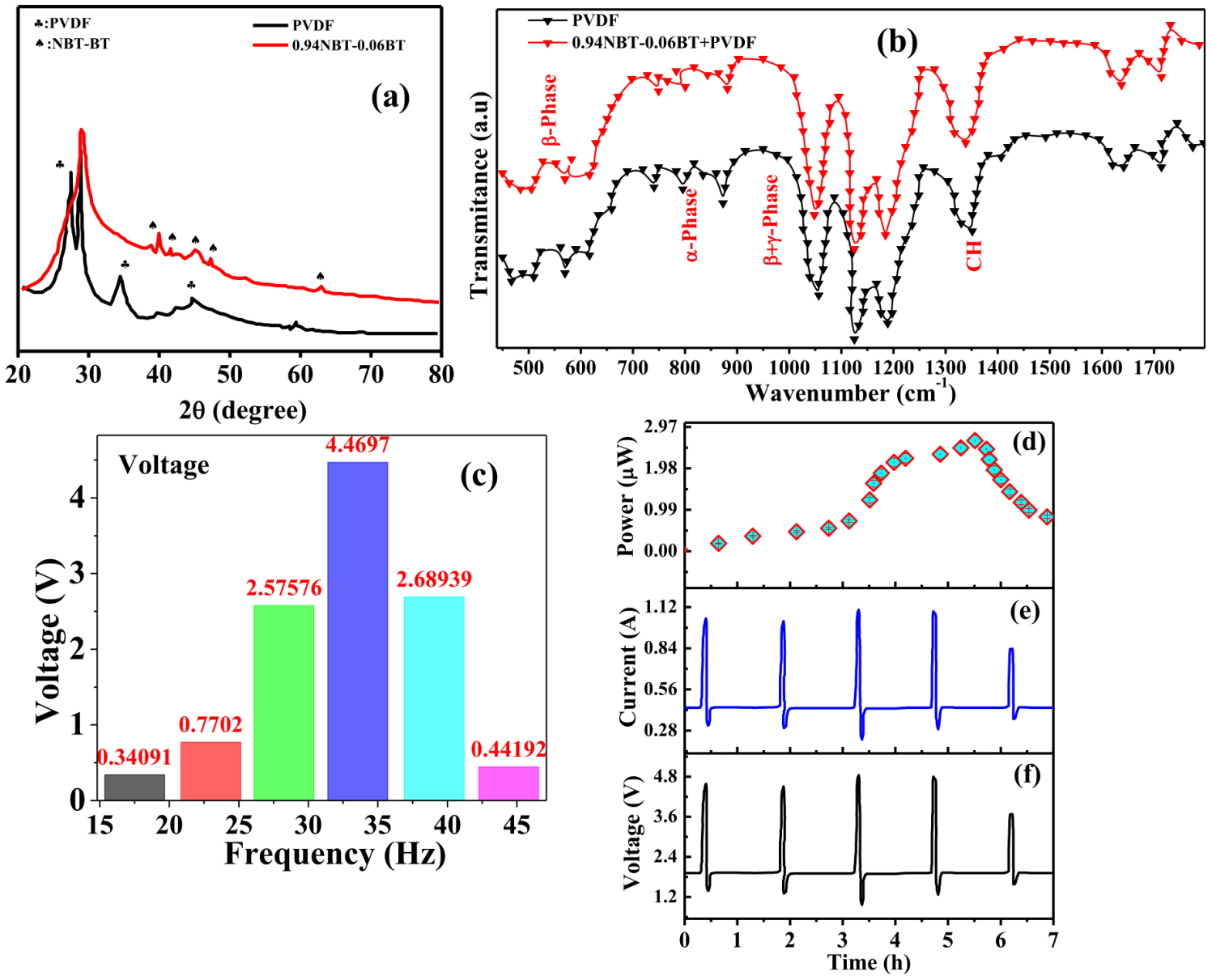


Figure 7

Energy harvesting performance of the 0.94NBT–0.06BT/PVDF composite, showing the generated open-circuit voltage and electrical output under mechanical vibration